Supplementary Information
Diffusion Coefficient in the ENAQT Regime Determined via the Velocity Autocorrelation Function Method

William Barford[a)]
[1)] *Department of Chemistry, Physical and Theoretical Chemistry Laboratory, University of Oxford, Oxford, OX1 3QZ, United Kingdom*
[2)] *Balliol College, University of Oxford, Oxford, OX1 3BJ, United Kingdom*

(Dated: 2 January 2026)

This Supplementary Information describes the failure of the velocity autocorrelation function method in the secular approximation (i.e., Eq. (32) of the main paper) to compute the diffusion coefficient deep within in the ENAQT regime. In particular we show that the velocity autocorrelation function method predicts a diffusion coefficient consistent with the definition that $D_{\rm ENAQT} \sim \Gamma \ell_{loc}^2$, where ℓ_{loc}^2 is the particle's Anderson localization length. Therefore, the temperature dependence of $D_{\rm ENAQT}$ is determined by the temperature dependence of Γ and ℓ_{loc}^2. This leads to the unphysical prediction that for $T < W_{\rm LGS}$, $D_{\rm ENAQT} \propto T$. Moreover, it fails to predict sub-diffusive dynamics, which has been observed experimentally and is predicted by the Redfield equation method.

Fig. 1 shows $D_\infty(T)$ calculated via the velocity autocorrelation function method for different values of disorder for the case $\Gamma = T$ (i.e., $\Gamma_0 = 1$). In all cases there is a low temperature ENAQT regime where $D_\infty(T) \propto \Gamma = T$, and a cross-over to a higher temperature quantum-Zeno regime where $D_\infty(T)$ follows the $\sigma = 0$ value (denoted by the black curve).

The crossover between the two regimes occurs when $D_{\rm ENAQT} \sim D_{\rm QZ}$, i.e., at $\Gamma(T) = V(T)/\ell_{\rm loc}(T)$. To understand the temperature dependence of this cross-over, we need to understand the temperature dependence of $\Gamma(T)$, $V(T)$ and $\ell_{\rm loc}(T)$. $\Gamma(T) = \Gamma_0 \times T$, while the temperature dependence of $\langle V^2 \rangle$ is shown in Fig. 2. The localization length, $\ell_{\rm loc}$, of the ath eigenstate can be determined by its participation number, ${\rm PN}_a$, defined as

$$ {\rm PN}_a = \left(\sum_n |\psi_a(n)|^4 \right)^{-1} . \tag{1} $$

The thermal averaged participation number, $\langle {\rm PN} \rangle = \sum_a P_a {\rm PN}_a$, is illustrated in Fig. 3.

Except for strong disorder, three distinct temperatures regimes can be identified in Fig. 2 and Fig. 3:

1. $T \le T_1 \sim W_{LGS} \sim \sigma^{4/3}$. In this regime only LGSs are thermally accessible and since the localization length of LGSs is only weakly energy-dependent, $\langle {\rm PN} \rangle$ is essentially independent of temperature. From the uncertainty principle, $\langle V^2 \rangle \propto \langle {\rm PN} \rangle^{-2}$ and thus $\langle V^2 \rangle$ is also independent of temperature.

2. $T_1 \le T \le T_2 \sim J$. In this regime the quasi-extended higher energy states (QES) become thermally accessible, equipartition is satisfied and thus $\langle V^2 \rangle = 2JT$. Since the localization length of QESs is energy-dependent, $\langle {\rm PN} \rangle$ also increases with temperature.

3. $T_2 \sim J \le T$. In this regime all states are thermally accessible and both $\langle {\rm PN} \rangle$ and $\langle V^2 \rangle$ are again independent of temperature. In particular, $\langle V^2 \rangle = 2J^2$ while $\langle {\rm PN} \rangle \propto \sigma^{-2}$.

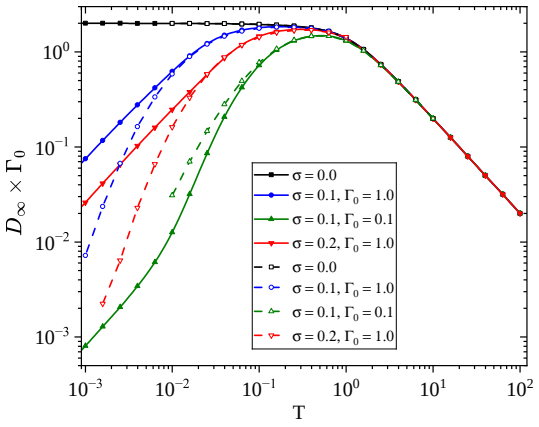

FIG. 1: The diffusion coefficient as a function of temperature for different values of the disorder, $\sigma' = \sigma/J$, and the dephasing factor, Γ_0 (where $\Gamma(T) = \Gamma_0 \times T$). ($k_B = \hbar = d = 1$.) Solid curves and filled symbols: results via the velocity autocorrelation function with chains of 400 sites and 200 realizations of the disorder. Note that since D_∞ is multiplied by Γ_0 the low temperature results using the velocity autocorrelation function method, for the same σ differ by a factor of Γ_0^2, whereas for all σ the high temperature results converge to the same value. Dashed curves and open symbols: results from quantum trajectories and the eigenstate thermalization hypothesis with chains of 400 sites and 10^5 quantum jumps.

[a)] Electronic mail: william.barford@chem.ox.ac.uk

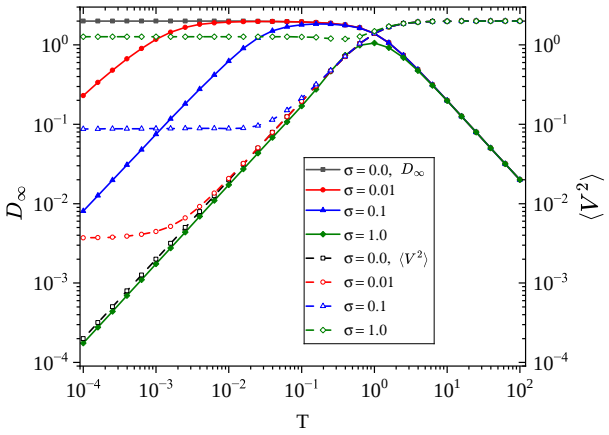

FIG. 2: Solid curves and filled symbols: the diffusion coefficient (via the velocity autocorrelation function method) as a function of temperature for different values of the disorder, $\sigma' = \sigma/J$. The dephasing factor$\Gamma_0 = 1$ (where $\Gamma(T) = \Gamma_0 \times T$). ($k_B = \hbar = d = 1$.) Dashed curves and open symbols: the mean-squared-speed, $\langle V^2 \rangle$. This indicates three temperature regimes with crossovers at T_1 and T_2, where $T_1 \sim W_{LGS} \sim \sigma^{4/3}$ and $T_2 \sim 1$. Here, for $\Gamma_0 = 1$, the ENAQT to quantum-Zeno crossover occurs at $T \sim T_1$.

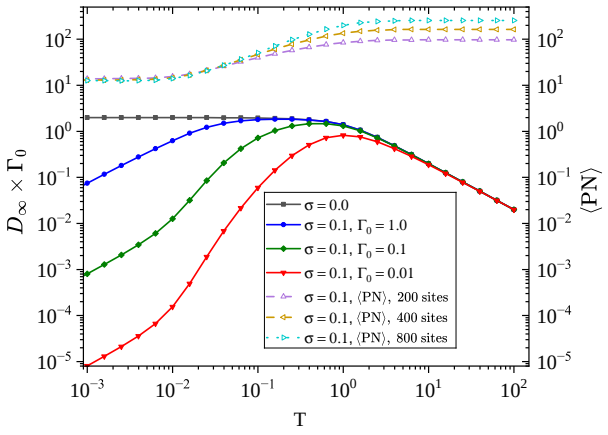

FIG. 3: Solid curves and filled symbols: the diffusion coefficient (via the velocity autocorrelation function method) as a function of temperature for different values of the dephasing factor Γ_0 (where $\Gamma(T) = \Gamma_0 \times T$). ($k_B = \hbar = d = 1$.) Dashed curves and open symbols: the thermal participation number, $\langle \mathrm{PN} \rangle$, which (as for $\langle V^2 \rangle$) indicates three temperature regimes. $\langle \mathrm{PN} \rangle$ converges slowly with the number of sites when $T > J$. For $\Gamma_0 < 1$ there are two sub-regimes in the ENAQT regime: (1) $T \leq T_1$, where D_{ENAQT} increases linearly with T and (2) $T_1 \leq T \leq T_3 \sim T_1/\Gamma_0$, where D_{ENAQT} increases superlinearly with T because of the temperature dependence of $\langle \mathrm{PN} \rangle$ caused by the thermal population of quasi-extended states.

For the case that $\Gamma_0 = 1$, it is apparent from Fig. 1 that the ENAQT to quantum-Zeno crossover occurs when $T \sim T_1$. The temperature-independent localization length in this regime therefore implies that $D_{\mathrm{ENAQT}}(T) = \Gamma(T)(\ell_{\mathrm{loc}}^{LGS})^2 \sim T$, as confirmed in Fig. 1.

The preceding discussion of the ENAQT to quantum-Zeno crossover applies to a large dephasing factor (i.e., $\Gamma_0 = 1$). For a smaller dephasing factor (i.e., $\Gamma_0 < 1$) the crossover occurs at the same dephasing value (i.e., the same value of $\Gamma = \Gamma_0 \times T$), but at a higher temperature. This means that there are now two sub-regimes in the ENAQT regime. To see this, recall that the ENAQT to quantum-Zeno crossover occurs at $\Gamma \sim V/\ell_{\mathrm{loc}}$, i.e., $T \sim V/\Gamma_0 \ell_{\mathrm{loc}} = T_1/\Gamma_0$. Thus, the two sub-regimes in the ENAQT regime are:

1. $T \leq T_1 \sim W_{LGS}$. In this regime only LGSs are thermally accessible and again $D_{\mathrm{ENAQT}} \sim T$.

2. $T_1 \leq T \leq T_3 = T_1/\Gamma_0$. In this regime the quasi-extended higher energy states become thermally accessible and hence $\langle \mathrm{PN} \rangle$ increases with temperature. Consequently, $D_{\mathrm{ENAQT}} \sim T \times f(T)$.

These predictions are confirmed in Fig. 3, which shows that D_{ENAQT} is a superlinear function of T for $T_1 \leq T \leq T_3$. Moreover, $T_3 \propto \Gamma_0^{-1}$.

Since $D_{\mathrm{ENAQT}} \sim \Gamma \ell_{loc}^2$ we expect that within the entire ENAQT regime (i.e., $T \leq T_3$), the ratio $D_\infty/\Gamma(T)\langle PN \rangle^2$ will be essentially constant. This is indeed confirmed by Fig. 4, which shows that this ratio is virtually constant over a temperature regime whose upper value $\propto \Gamma_0^{-1}$.

Finally, we return to predictions obtained using the eigenstate thermalization hypothesis (ETH). These are illustrated in Fig. 1. As already discussed in the main paper, for translationally invariant systems, the ETH prediction agrees precisely by using the velocity autocorrelation function. For disordered systems, the two are in good agreement for $T > 0.1$, but at lower temperatures their predictions begin to deviate. At $T \sim 0.01$ the predictions differ by a factor of ~ 2, while at even lower temperatures they begin to differ significantly. The origin of this deviation can be traced to the failure of the ETH in disordered systems at low temperatures, as described in Section II.B.2 and illustrated in Fig. 2 of the main paper. Crucially, however, for different values of disorder, σ, and dephasing factors, Γ_0, both methods predict the same qualitative behavior and there is quantitative agreement on the temperature of the ENAQT to quantum-Zeno crossover.

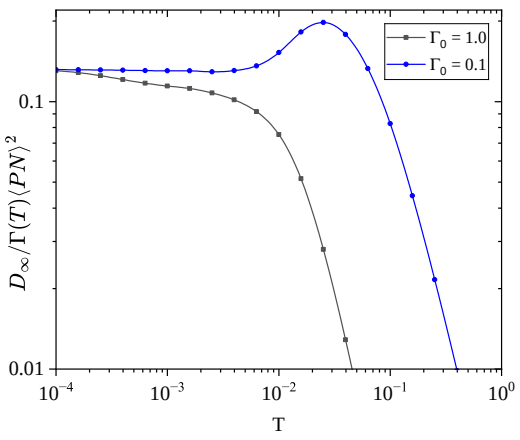

FIG. 4: The ratio $D_\infty/\Gamma(T)\langle PN\rangle^2$ is essentially constant in the ENAQT regime. ($k_B = \hbar = d = 1$.) When the dephasing factor $\Gamma_0 = 1$, the regime spans $0 \leq T \leq T_1 \sim W_{LGS} \sim \sigma^{4/3}$. $T_1/J \sim 10^{-2}$ when $\sigma/J = 0.1$. When the dephasing factor $\Gamma_0 < 1$ the ENAQT regime spans $0 \leq T \leq T_3 = T_1/\Gamma_0$. $T_3/J \sim 10^{-1}$ when $\sigma/J = 0.1$ and $\Gamma_0 = 0.1$.

In conclusion, we have shown in this SI that the velocity autocorrelation function method is unreliable deep within the ENAQT regime. Conversely, the weak-coupling Redfield equation method becomes unreliable at the ENAQT-QZ cross-over, because as shown in Fig. 4 of the main paper, at the crossover it predicts a value for D exceeding the value for a uniform system, namely, $D = \langle V^2\rangle/\Gamma$.